

Chapter 29

Structural Study of the Modified $\text{Cu}_{0.4}\text{Co}_{0.4}\text{Ni}_{0.4}\text{Mn}_{1.8}\text{O}_4$ and $\text{Cu}_{0.1}\text{Ni}_{0.8}\text{Co}_{0.2}\text{Mn}_{1.9}\text{O}_4$ Ceramics Using Combined Methods



H. Klym, I. Hadzaman, A. Ingram, O. Shpotyuk, I. Karbovnyk, Yu. Kostiv,
I. Vasylyshyn, and D. Chalyy

29.1 Introduction

Temperature-sensitive spinel ceramics based on transition metal manganites with topologically disordered structures is one of the perspective materials for temperature sensors and other practical applications [1–3]. The main structural elements in these materials are grain, grain boundaries, and pores depending on technological procedure of ceramic sintering [4, 5]. Understanding of correlation between grain-porous and free-void structures as well as physical properties of such materials is still in focus of scientific and commercial interests for scientists across the globe [6, 7].

In ceramics, depending on the sintering temperature, shrinkage of the atomic structure occurs, eventually leading to more or less complex pore topology [8–10].

H. Klym (✉) · Y. Kostiv · I. Vasylyshyn
Lviv Polytechnic National University, Lviv, Ukraine
e-mail: halyna.i.klym@lpnu.ua

I. Hadzaman
Drohobych State Pedagogical University, Drohobych, Ukraine

A. Ingram
Opole University of Technology, Opole, Poland

O. Shpotyuk
Vlokh Institute of Physical Optics, Lviv, Ukraine

Jan Dlugosz University in Czestochowa, Czestochowa, Poland

I. Karbovnyk
Ivan Franko National University of Lviv, Lviv, Ukraine

D. Chalyy
Lviv State University of Life Safety, Lviv, Ukraine

These pores along with specific vacancy-type defects within individual crystalline grains and grain boundaries represent free-volume structure of ceramics. In addition, previous investigations have shown that in temperature-sensitive spinel-type ceramics, the quantity of the additional phase and its distribution in bulk and on the surface of ceramic samples are essentially influenced by temperature-time sintering regimes [5, 11].

But technological modification of spinel ceramics results in stabilization of functional properties of ceramics. So, in $\text{Cu}_{0.1}\text{Ni}_{0.8}\text{Co}_{0.2}\text{Mn}_{1.9}\text{O}_4$ ceramics, metallic additives located in intergranular regions closely to grain boundaries diminish thermally activated aging phenomena owing by stabilizing the cationic distribution within individual ceramic grains. As a result, the chemically modified ceramics show higher stability in comparison with non-modified ones [4, 12].

Because of significant complications in the structure of spinel-type ceramics revealed at the levels of individual grains, grain boundaries, and pores [13], the further progress in this field is dependent to a great extent on the development of new characterization techniques, which can be used in addition to traditional ones (scanning/tunneling electron microscopy, porosimetry methods, etc.). This concerns, in part, the positron annihilation lifetime (PAL) spectroscopy, the alternative method only recently applied to fine-grained powders, nanostructured glasses, and ceramics [14, 15]. In general, the PAL reflects a so-called free-volume distribution within structural network of solids.

It was shown previously [16–18] that in the case of ceramics, PAL data are determined mainly by crystallographic features of individual grains, while structural disturbances due to grain contacts inside ceramics were a subject for additional complications. This is why the measured positron lifetime spectra for sintered ceramics can be adequately explained within a unified positron annihilation model involving discrete positron trapping and ortho-positronium (*o-Ps*) decay modes, the best fitting being achieved using at least three independent components in the resolved lifetime spectra (two for positron trapping and one for *o-Ps* decaying) [11, 16–19]. In terms of this model, the second positron trapping component with lifetime τ_2 is attributed to free-volume defects such as neutral or negatively charged vacancies especially near grain boundaries. The shortest component named the reduced bulk positron lifetime τ_1 is mainly due to annihilation in defect-free bulk with small mixing from other positron trapping channels. The largest component at the level of a few nanoseconds is responsible for a so-called *o-Ps* “pick-off” annihilation [18, 20].

The main aim of this work is structural study of the technologically modified $\text{Cu}_{0.4}\text{Co}_{0.4}\text{Ni}_{0.4}\text{Mn}_{1.8}\text{O}_4$ and $\text{Cu}_{0.1}\text{Ni}_{0.8}\text{Co}_{0.2}\text{Mn}_{1.9}\text{O}_4$ ceramics using alternative PAL technique in comparison with scanning electron microscopy (SEM) and porosimetry methods [8, 21].

29.2 Preparation of Modified Ceramics

Macro- and micro-modified $\text{Cu}_{0.4}\text{Co}_{0.4}\text{Ni}_{0.4}\text{Mn}_{1.8}\text{O}_4$ ceramics was obtained via traditional ceramic technology as was described in greater details elsewhere [4, 12, 16, 20, 22]. Equal molar amounts of initial powders were mixed in a planetary ball mill for 96 h in an environment with acetone to obtain mixture. The aqueous solution of polyvinyl alcohol was used for obtaining of the molding powder. Bilateral compression was performed in steel molds. After pressing these samples were sintered in a furnace at maximal temperature (T_s) 1100 °C for 2 h. To validate PAL investigations performed, we divided the $\text{Cu}_{0.4}\text{Co}_{0.4}\text{Ni}_{0.4}\text{Mn}_{1.8}\text{O}_4$ ceramics into two groups presumably not affecting lifetime spectra – the $\text{Cu}_{0.4}\text{Co}_{0.4}\text{Ni}_{0.4}\text{Mn}_{1.8}\text{O}_4$ -micro- and $\text{Cu}_{0.4}\text{Co}_{0.4}\text{Ni}_{0.4}\text{Mn}_{1.8}\text{O}_4$ -macro-modified ceramics prepared by preliminary sifting of powder through fine (with 0.1 mm pores) and more rough sieve (0.5 mm pores). In both cases, the sizes of intrinsic pores are too large to change significantly positron annihilation spectra [20].

To preparation of $\text{Cu}_{0.1}\text{Ni}_{0.8}\text{Co}_{0.2}\text{Mn}_{1.9}\text{O}_4$ ceramics, the precise amounts of high purity and previously tested carbonate salts were weighted and wet mixed. This mixture was thermally decomposed in the air at $700 \pm 5^\circ\text{C}$ for 4 h [12, 16]. Then the obtained powders were milled, blended with organic binder, and pressed into the disks of approximately 10 mm in diameter and 1 mm in thickness. The prepared four batches of blanks were sintered in the air in respect to the time-temperature regimes (see Fig. 29.1).

It should be noted the sintering route of ceramics was performed to ensure all necessary conditions for inhibition effect in degradation [23], the content of additional NiO phase with NaCl-type structure having decisive role in the final ceramic structure. In fact, we deal with Ni-deficient ceramics in respect to stoichiometric $\text{Cu}_{0.1}\text{Ni}_{0.8}\text{Co}_{0.2}\text{Mn}_{1.9}\text{O}_4$ composition taken as start one in disproportionality

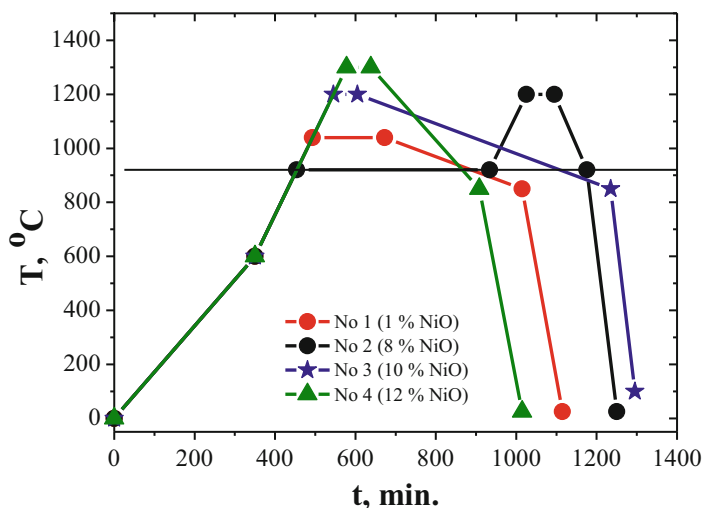


Fig. 29.1 Time-temperature sintering regime for $\text{Cu}_{0.1}\text{Ni}_{0.8}\text{Co}_{0.2}\text{Mn}_{1.9}\text{O}_4$ ceramics [16]

calculations. Four batches of $\text{Cu}_{0.1}\text{Ni}_{0.8}\text{Co}_{0.2}\text{Mn}_{1.9}\text{O}_4$ ceramics with 1–12% of NiO phase were prepared owing to different amounts of thermal energy transferred during the sintering (batch No. 1–1% NiO, batch No. 2–8% NiO, batch No. 3–10% NiO, batch No. 4–12% NiO). The latter was numerically determined as square value restricted by temperature-time curve above straight line corresponding to 920 °C, which is the temperature of monophase $\text{Cu}_{0.1}\text{Ni}_{0.8}\text{Co}_{0.2}\text{Mn}_{1.9}\text{O}_4$ ceramic formation [16, 23].

29.3 Experimental Details

Structures of grains, grain boundaries, and pores for micro- and macro-modified $\text{Cu}_{0.4}\text{Co}_{0.4}\text{Ni}_{0.4}\text{Mn}_{1.8}\text{O}_4$ ceramics were studied using LEO 982 microscope [20, 24]. Pore size distribution in the region from 2 to 300 nm was investigated with Hg-porosimetry (POROSIMETR 4000) [11, 20, 21].

Microstructure of the $\text{Cu}_{0.1}\text{Ni}_{0.8}\text{Co}_{0.2}\text{Mn}_{1.9}\text{O}_4$ ceramics was probed using electron microscope JSM-6700F, cross sections morphology of the samples being tested near surface (0–70 μm depth) and chip centers.

PAL measurements for all samples of ceramics were performed using ORTEC spectrometer at temperature of 20 °C and relative humidity of ~35% [11, 16–18, 25]. The isotope ^{22}Na was used as positron source. The two identical samples of ceramics were placed in the both sides of the source. The PAL spectra were treated by LT computer program [26]. For each pair of ceramic samples, we used three measured positron annihilation spectra. The best results were obtained at three-component fitting procedure with parameters of each components (τ_1, I_1) , (τ_2, I_2) , and (τ_3, I_3) for micro- and macro-modified $\text{Cu}_{0.4}\text{Co}_{0.4}\text{Ni}_{0.4}\text{Mn}_{1.8}\text{O}_4$ ceramics and two-component component fitting procedure with parameters (τ_1, I_1) , (τ_2, I_2) . Such parameters as average positron lifetimes τ_{av} , positron lifetime in defect-free bulk τ_{b} , and positron trapping rate in defects κ_{d} were calculated using two-state positron trapping model [26, 27]. The difference $(\tau_2 - \tau_{\text{b}})$ can be accepted as a size measure of extended defects where positrons are trapped, and the τ_2/τ_{b} ratio represents the nature of these defects [28].

29.4 Results and Discussion

29.4.1 *Micro- and Macro-modified $\text{Cu}_{0.4}\text{Co}_{0.4}\text{Ni}_{0.4}\text{Mn}_{1.8}\text{O}_4$ Ceramics*

According to our X-ray diffraction investigations, the micro- and macro-modified $\text{Cu}_{0.4}\text{Co}_{0.4}\text{Ni}_{0.4}\text{Mn}_{1.8}\text{O}_4$ ceramics are preferentially of single spinel phase with lattice parameter of $a = 8.365 \text{ \AA}$ [4, 20]. The XRD patterns for the micro- and macro-modified $\text{Cu}_{0.4}\text{Co}_{0.4}\text{Ni}_{0.4}\text{Mn}_{1.8}\text{O}_4$ ceramics are shown in Figs. 29.2 and 29.3.

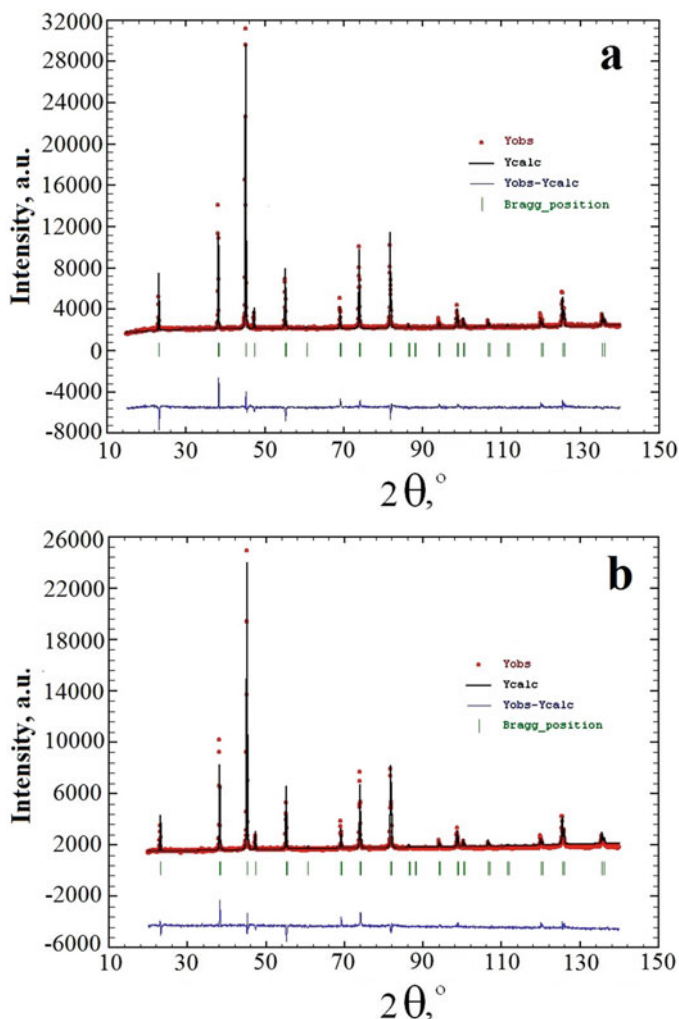


Fig. 29.2 Experimental (rings), theoretical (line), and difference XRD pattern (down) for micro- (a) and macro-modified (b) $\text{Cu}_{0.4}\text{Co}_{0.4}\text{Ni}_{0.4}\text{Mn}_{1.8}\text{O}_4$ ceramics (row of reflexes is the basic spinel phase)

In respect to SEM investigations, the $\text{Cu}_{0.4}\text{Co}_{0.4}\text{Ni}_{0.4}\text{Mn}_{1.8}\text{O}_4$ ceramics contained large grains (~ 10 mm) as well as relatively sharp grain boundaries. So-called “closed” pores have a spherical form and are located mainly near grain boundaries. As it is obvious from electron micrographs (Fig. 29.4), micro- and macro-modified $\text{Cu}_{0.4}\text{Co}_{0.4}\text{Ni}_{0.4}\text{Mn}_{1.8}\text{O}_4$ ceramics differ only by pores [20]. The neatly shaping grains with comparatively tiny pores (~ 1 mm) are characteristic for micro-modified $\text{Cu}_{0.4}\text{Co}_{0.4}\text{Ni}_{0.4}\text{Mn}_{1.8}\text{O}_4$ samples, while macro-modified $\text{Cu}_{0.4}\text{Co}_{0.4}\text{Ni}_{0.4}\text{Mn}_{1.8}\text{O}_4$ ceramics contain similar crystalline grains with larger pores (reaching in size up to ~ 10 mm).

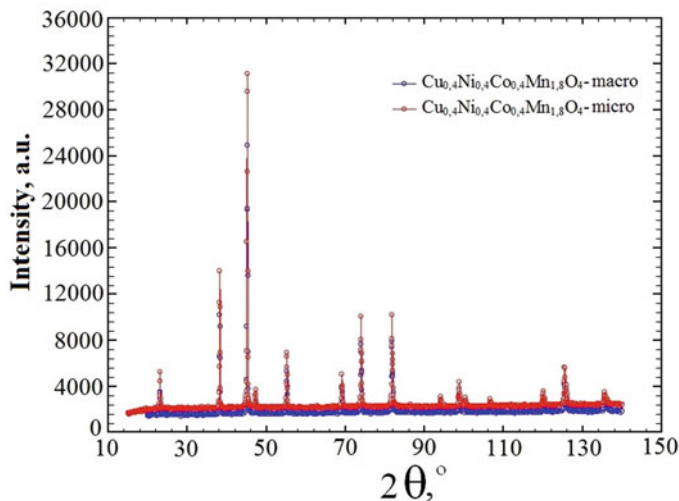


Fig. 29.3 Comparison of experimental XRD patterns for crystalline phase of micro- (a) and macro-modified (b) $\text{Cu}_{0.4}\text{Co}_{0.4}\text{Ni}_{0.4}\text{Mn}_{1.8}\text{O}_4$ ceramics

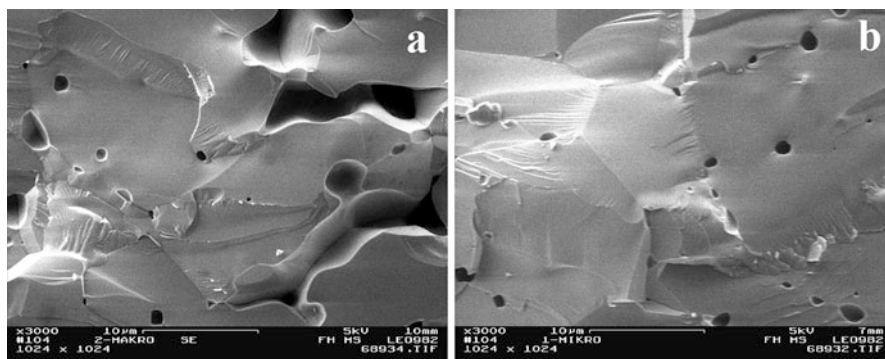


Fig. 29.4 Scanning electron micrographs for micro- (a) and macro-modified (b) $\text{Cu}_{0.4}\text{Co}_{0.4}\text{Ni}_{0.4}\text{Mn}_{1.8}\text{O}_4$ ceramics

Open pore size distributions for micro- and macro-modified $\text{Cu}_{0.4}\text{Co}_{0.4}\text{Ni}_{0.4}\text{Mn}_{1.8}\text{O}_4$ ceramics are shown in Fig. 29.5. Such distributions cover significant amount of charge-transferring nanopores depending on sintering procedure and small amount of communication mesopores [11, 20]. In contrast to humidity-sensitive MgAl_2O_4 ceramics, temperature-sensitive $\text{Cu}_{0.4}\text{Co}_{0.4}\text{Ni}_{0.4}\text{Mn}_{1.8}\text{O}_4$ ceramics practically do not possess outside-delivering macropores depending on specific surface area of initial powder [5]. Thus, $\text{Cu}_{0.4}\text{Co}_{0.4}\text{Ni}_{0.4}\text{Mn}_{1.8}\text{O}_4$ ceramics prepared at 1100 °C exhibit so-called one-modal pore size distribution with maximum position near 2 nm and double-maximum near 2.3 and 5.5 nm for

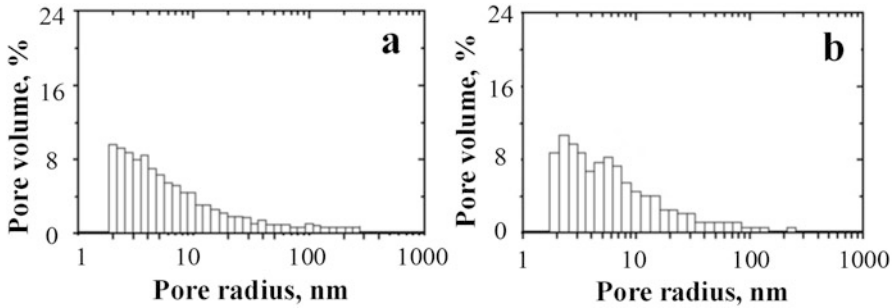


Fig. 29.5 Pore size distributions of micro- (a) and macro-modified (b) $\text{Cu}_{0.4}\text{Co}_{0.4}\text{Ni}_{0.4}\text{Mn}_{1.8}\text{O}_4$ ceramics

micro- and macro-modified $\text{Cu}_{0.4}\text{Co}_{0.4}\text{Ni}_{0.4}\text{Mn}_{1.8}\text{O}_4$ ceramics, respectively (Fig. 29.5).

Let's try to discuss the results (Table 29.1) obtained within positron trapping model by accepting that structural peculiarities of spinel ceramics are associated mainly in the first PAL component (τ_1, I_1). The second component (τ_2, I_2) corresponds directly to free-volume positron traps (voids in the form of vacancy-like clusters, agglomerates, etc.) located near grain boundaries [11, 16, 20]. It means that input of the first component in the PAL spectra will be, in part, a determinant of the average electron density distribution reflected structural compactness of the testes network. The τ_2 lifetime is associated with the size of voids and the intensity I_2 is proportional to the amount of voids in the case of the same defect-free bulk annihilation lifetime [16, 20]. The third component (τ_3, I_3) corresponds to *o-Ps* annihilation in nanopores. In spite of small value of I_3 intensity (2%), this component cannot be removed without losses in the quality of the fitting procedure. The similar component was detected in many porous materials with different structural type [16, 29]. In addition, the third component can be related with *o-Ps* "pick-off" annihilation in water absorbed by materials [29]. We don't exclude the meaning of other positron annihilation channels in this PAL component too, such as para-positronium (*p-Ps*) decaying with character lifetime of 0.125 ns [14]. But their influence is negligibly small, if the above requirement on close positron affinity will be more or less kept within a whole positron trapping medium [30].

As it was shown in Tables 29.1 and 29.2, micro- and macro-modification of $\text{Cu}_{0.4}\text{Co}_{0.4}\text{Ni}_{0.4}\text{Mn}_{1.8}\text{O}_4$ ceramics during preparation does not influence their fitting parameters. As a result, such positron trapping modes as positron lifetime τ_b , average positron lifetime $\tau_{av.}$, positron trapping rate of defect κ_d , size of extended defects, where positrons are trapped ($\tau_2 - \tau_b$), and ratio represents the nature of these defects (τ_2/τ_b) [14, 21] remain unchanged. Obviously, pores of large examination by SEM and Hg-porosimetry do not modify significantly the measured positron lifetime spectra, testifying in a favor of correctness of the performed measuring and fitting procedures.

Table 29.1 Fitting parameters of LT computer program describing positron annihilation in the micro- and macro-modified $\text{Cu}_{0.4}\text{Co}_{0.4}\text{Ni}_{0.4}\text{Mn}_{1.8}\text{O}_4$ ceramics

Sample	Fitting parameters						Component input		
	τ_1 , ns	I_1 , a.u.	τ_2 , ns	I_2 , a.u.	τ_3 , ns	I_3 , a.u.	$\tau_1 I_1$, ns	$\tau_2 I_2$, ns	$\tau_3 I_3$, ns
$\text{Cu}_{0.4}\text{Co}_{0.4}\text{Ni}_{0.4}\text{Mn}_{1.8}\text{O}_4$ (macro)	0.21	0.78	0.37	0.20	1.85	0.02	0.16	0.07	0.04
$\text{Cu}_{0.4}\text{Co}_{0.4}\text{Ni}_{0.4}\text{Mn}_{1.8}\text{O}_4$ (micro)	0.22	0.77	0.38	0.21	1.83	0.02	0.17	0.08	0.04

Table 29.2 Positron trapping modes in the micro- and macro-modified $\text{Cu}_{0.4}\text{Co}_{0.4}\text{Ni}_{0.4}\text{Mn}_{1.8}\text{O}_4$ ceramics calculated within two-state positron trapping model and free-volume characteristics

Sample	Free-volume characteristics			Positron trapping modes				
	R_{octa} , Å	R_{tetra} , Å	R (Tao-Eldrup), nm	τ_{av} , ns	τ_{b} , ns	κ_{d} , ns ⁻¹	$\tau_2 - \tau_{\text{b}}$, ns	τ_2/τ_{b}
$\text{Cu}_{0.4}\text{Co}_{0.4}\text{Ni}_{0.4}\text{Mn}_{1.8}\text{O}_4$ (macro)	0.69	0.64	2.74	0.24	0.23	0.4	0.14	1.6
$\text{Cu}_{0.4}\text{Co}_{0.4}\text{Ni}_{0.4}\text{Mn}_{1.8}\text{O}_4$ (micro)			2.72	0.25	0.24	0.4	0.14	1.6

As was shown early in [20], the potential positron traps in functional spinel-type ceramics are tetrahedral and octahedral cation vacancies. The average volume of these tetrahedrons V_{tetra} and octants V_{octa} can be selected as free-volume parameters for spinel-structured ceramics.

The radii of tetrahedral and octahedral sites in a spinel structure can be calculated using lattice parameter a [20]:

$$R_{\text{tetra}} = \sqrt{3} \left(u - \frac{1}{4} \right) a - R_0, \quad (29.1)$$

$$R_{\text{octa}} = \left(\frac{5}{8} - u \right) a - R_0 \quad (29.2)$$

where u is oxygen parameter and R_0 is oxygen atom with radius of 1.32 Å.

The oxygen parameter u in oxide spinels is near 0.385 and insignificantly depends on cation type [4, 16]. The radius of tetrahedral vacancies in $\text{Cu}_{0.4}\text{Co}_{0.4}\text{Ni}_{0.4}\text{Mn}_{1.8}\text{O}_4$ ceramics is 0.64 Å, which gives V_{tetra} in spherical approximation $\sim 1.10 \text{ \AA}^3$. The volume of octahedral vacancies V_{octa} is $\sim 1.37 \text{ \AA}^3$.

As it was noted [20], positrons have a preference to annihilate in octahedral vacancy sites as it follows from charge density distribution in partially inverted spinel structures. But the calculated ratio between the first component inputs in the PAL spectra for previously studied MgAl_2O_4 ceramics [20, 31] and $\text{Cu}_{0.4}\text{Co}_{0.4}\text{Ni}_{0.4}\text{Mn}_{1.8}\text{O}_4$ ceramics (0.78) is closer to the ratio between corresponding volumes of tetrahedral vacancies (0.76) rather than octahedral ones (0.69). Consequently, in the studied $\text{Cu}_{0.4}\text{Co}_{0.4}\text{Ni}_{0.4}\text{Mn}_{1.8}\text{O}_4$ ceramics in contrast to nanocrystalline ferrites [14], positron trapping in tetrahedral vacancies predominates in the first PAL component. The positron trapping in octahedral vacancies is character to inverse spinel structure.

It is evident that octahedral monovacancies themselves do not play a decisive role in the second component of PAL spectra. This component is associated with more extended agglomerates such as vacancy-like clusters and nanovoids. They appear, as a rule, near grain boundaries, where ceramic structure is more defective. The characteristic volumes of these clusters are larger in ceramics with a more stretched pore structure. In seats where ceramics are composed of very small grains with divaricated grain boundaries and tiny pores, the positrons are prepped more effective.

Recently, PAL spectroscopy started to be used as an alternative porosimetry technique to characterize the local free volumes first of all in both open and closed nanopores [14, 32, 33–35]. The PAL method is particularly effective when P_s is formed. In disordered solids, P_s is usually organized in two ground states (p - P_s and o - P_s) and localized in the pores and free volumes [33–35]. Usually, quantification is based on the analysis of o - P_s lifetime (the lifetimes of the third component τ_3 in $\text{Cu}_{0.4}\text{Co}_{0.4}\text{Ni}_{0.4}\text{Mn}_{1.8}\text{O}_4$ ceramics correspond to o - P_s lifetime). The o - P_s “pick-off” annihilation depends on the size of holes and gives additional important information on the void structure of the materials [35]. Despite small I_3 intensity for $\text{Cu}_{0.4}\text{Co}_{0.4}\text{Ni}_{0.4}\text{Mn}_{1.8}\text{O}_4$ ceramics, it is possible to estimate the average nanopore size from o - P_s lifetime in a given material [51]. Assuming approximately spherical shape of the free volume, the o - P_s lifetime (τ_{o-P_s}) in oxide materials can be related to the average radius of pores (R) by semiempirical Tao-Eldrup equation [36, 37]:

$$\tau_{o-P_s} = \left[2 \left(1 - \frac{R}{R + \Delta R} + \frac{1}{2\pi} \sin \left(\frac{2\pi R}{R + \Delta R} \right) \right) + 0.007 \right]^{-1}, \quad (29.3)$$

where ΔR is the empirically determined parameter (in the classical case $\Delta R \approx 0.1656$ nm), describing effective thickness of the electron layer responsible for the “pick-off” annihilation of o - P_s in the pore [36, 37].

In functional $\text{Cu}_{0.4}\text{Co}_{0.4}\text{Ni}_{0.4}\text{Mn}_{1.8}\text{O}_4$ ceramics, there is one o - P_s PAL component with small intensity (2%). Therefore, τ_3 lifetime can be related to corresponding pores via Tao-Eldrup model. The τ_{o-P_s} value of around ~ 1.8 ns (τ_3 in Table 29.1) corresponds to nanopores with radius (R) distribution centered near ~ 0.27 nm. This result is addition to Hg-porosimetry measurements. In addition, it should be noted that porosimetry methods are limited to open pores, which should have an

access to the environment to be determined. On the other hand, PAL spectroscopy can probe both open and closed pores in functional oxide ceramics of sizes ranging from atomic scale to several tens of nanometers.

29.4.2 Technologically Modified $\text{Cu}_{0.1}\text{Ni}_{0.8}\text{Co}_{0.2}\text{Mn}_{1.9}\text{O}_4$ Ceramics

In respect to the results of microstructure characterization with X-ray diffractometry method, the lattice constant of the main spinel was slightly grown from 8.38 до 8.41 Å without significant changes in the parameter of additional NiO phase (at the level of 4.17–4.19 Å) despite increase in the content of this phase from 1 to 12% [16].

To explain the above phenomena, microstructure of the prepared ceramics was studied. As it follows from Fig. 29.6, the prepared ceramic samples differ significantly by their grain-pore microstructure.

The samples of batch No. 1 (Fig. 29.6a) are characterized by fine 1–3 μm grains. The numerous intergranular pores are small enough in these samples, their sizes not exceeding 1–2 μm. White film, which can be attributed to additional NiO phase extractions, weakly appears in these ceramics mainly near intergrain boundaries; sometimes it partially fills of pores. The samples of batch No. 2 (Fig. 29.6a) are characterized by larger grains with sizes near 5–7 μm, some of them achieving 10 μm. The white NiO film appears in these ceramics only in the regions of grain boundaries. The grain structure of the samples of batch No. 3 (Fig. 29.6c) gradually changes. The corresponding chip structure of these ceramics is more monolithic, it being characterized only by separate pores with 1–3 μm in sizes. White NiO film appears as bright layer of 10 μm thickness on the grain surface of these samples. In contrast, the grain structure of the samples of batch No. 4 (Fig. 29.6d) attains fully monolithic shape. Only some individual pores of relatively large sizes (near 3–5 μm) are observed in these ceramics, the NiO appearing as uniform layer on the whole ceramic surface. The observed additional NiO phase is nonuniformly distributed within ceramic bulk, being more clearly pronounced near grain boundaries. These phase extractions serve as specific trapping centers for positrons penetrating ceramics.

Investigation of element composition of grain for $\text{Cu}_{0.1}\text{Ni}_{0.8}\text{Co}_{0.2}\text{Mn}_{1.9}\text{O}_4$ ceramics specifies on their stoichiometry (Fig. 29.7). However basic influence on the structural processes in material open and closed pores formed by modification on the stage of sintering is realized.

By accepting two-state positron trapping model [27, 28], for spinel-type ceramic materials, the first component of spectra was connected with main spinel structure and the second one – with extended defects located near grain boundaries in the vicinity of additional extracted phases. The intensity I_1 corresponds to the amounts

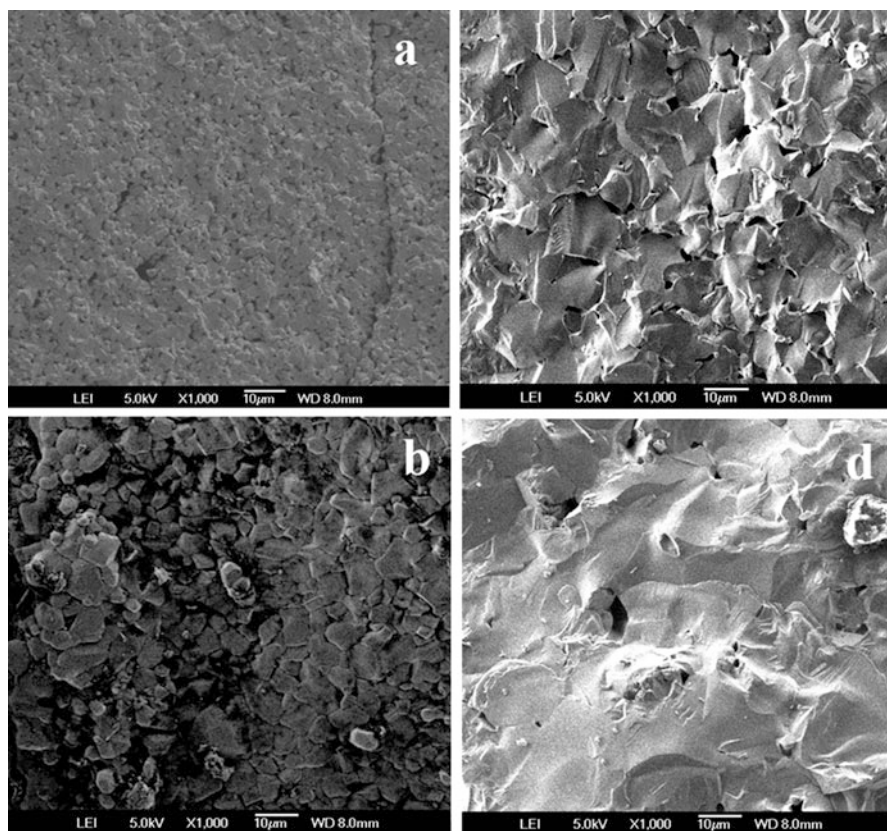


Fig. 29.6 Microstructure of modified $\text{Cu}_{0.1}\text{Ni}_{0.8}\text{Co}_{0.2}\text{Mn}_{1.9}\text{O}_4$ ceramics: (a) batch No 1 (1 % NiO), (b) batch No 2 (8 % NiO), (c) batch No 3 (10 % NiO), (d) batch No 4 (12 % NiO)

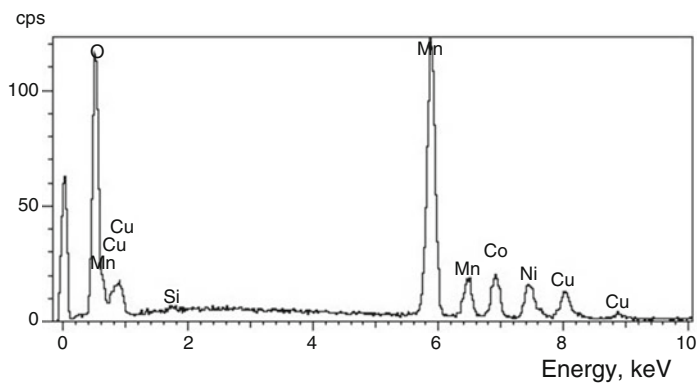


Fig. 29.7 Elemental composition of grain for $\text{Cu}_{0.1}\text{Ni}_{0.8}\text{Co}_{0.2}\text{Mn}_{1.9}\text{O}_4$ ceramics

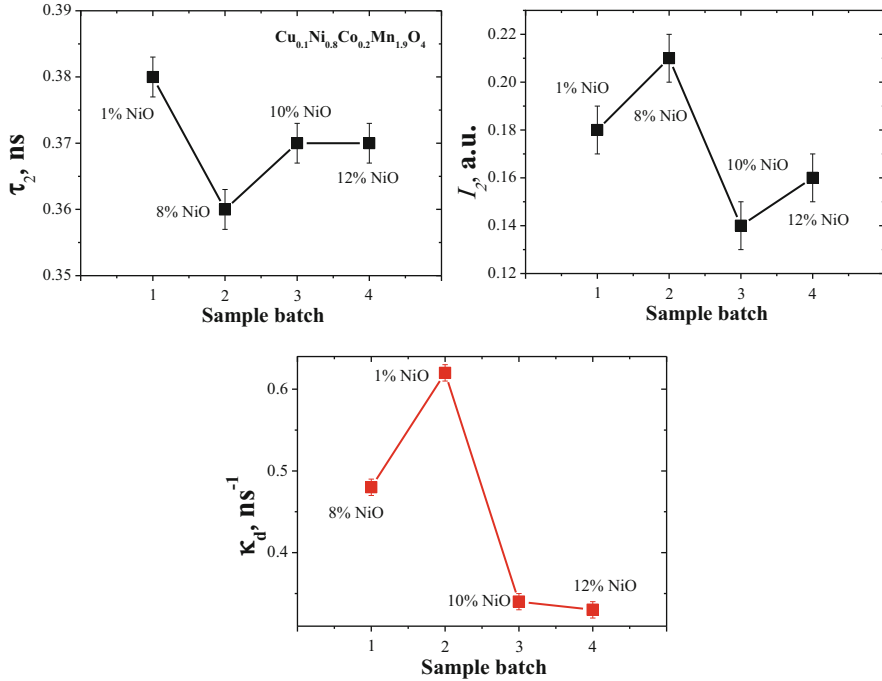


Fig. 29.8 Defect-related component and positron trapping rate in defects as a function of amount of NiO in the studied $\text{Cu}_{0.1}\text{Ni}_{0.8}\text{Co}_{0.2}\text{Mn}_{1.9}\text{O}_4$ ceramics

of the main spinel phase, while the I_2 intensity to the amount of addition NiO phase near grain boundaries.

The lifetime of the first and second components for $\text{Cu}_{0.1}\text{Ni}_{0.8}\text{Co}_{0.2}\text{Mn}_{1.9}\text{O}_4$ ceramics is typically for spinel-structured materials and equals ~ 0.37 and 0.20 ns, accordingly (Table 29.3). The lower τ_1 value in the batch No. 2 (0.17 ns) will be correlated with Ni content in different crystallographic positions. Since the amount of grain/pores in the sample of batch No. 2 was greater, the process of positron trapping in these ceramics was more intensive (the positron trapping rate of defects increased from 0.48 to 0.62 ns^{-1}).

The intensity of the second component for samples of batch No. 1 is 18% (Table 29.3, Fig. 29.8), although amount of additional NiO phase in this batch is small (1%). This additional phase is localized near grain boundaries and partly fills pores. In samples of batch No. 2, the intensity I_2 increases to 21% correspondingly to amount of NiO phase.

In batch No. 3 ceramics, the grain-pore structure was not developed because of occurred monolithization process accompanied by surface extraction of additional NiO phase. The same was character for batch No. 4 ceramic samples.

Table 29.3 PAL characteristics of $\text{Cu}_{0.4}\text{Co}_{0.4}\text{Ni}_{0.4}\text{Mn}_{1.8}\text{O}_4$ ceramic mathematical treatment within two-component fitting procedure

Sample batch	Fitting parameters			Component input			Positron trapping modes				
	τ_1 , ns	I_1 , a.u.	τ_2 , ns	I_2 , a.u.	$\tau_{av.}^1$, ns	$\tau_{av.}^2$, ns	$\tau_{av.}$, ns	τ_b , ns	κ_d , ns ⁻¹	$\tau_2 - \tau_b$, ns	τ_2/τ_b
No. 1	0.19	0.82	0.38	0.18	0.16	0.07	0.23	0.21	0.48	0.17	1.8
No. 2	0.17	0.79	0.36	0.21	0.14	0.07	0.21	0.19	0.62	0.17	1.9
No. 3	0.20	0.86	0.37	0.14	0.17	0.05	0.22	0.21	0.34	0.16	1.7
No. 4	0.21	0.84	0.37	0.16	0.18	0.06	0.23	0.22	0.33	0.15	1.7

These transformations were in good agreement with positron trapping rate in defects (Table 29.3, Fig. 29.8). Nevertheless, there were no significant changes in τ_{av} , τ_b , τ_2/τ_b , and $(\tau_2 - \tau_b)$. In all cases, the same type of positron trapping center is formed. The character size of these extended positron traps near grain boundaries estimated due to $(\tau_2 - \tau_b)$ difference is close to single-double atomic vacancies [16].

29.5 Conclusions

Structural peculiarities of temperature-sensitive $\text{Cu}_{0.4}\text{Co}_{0.4}\text{Ni}_{0.4}\text{Mn}_{1.8}\text{O}_4$ ceramics caused by micro- and macro-modifications as well as $\text{Cu}_{0.1}\text{Ni}_{0.8}\text{Co}_{0.2}\text{Mn}_{1.9}\text{O}_4$ ceramics related with monolithization processes were studied using traditional structural methods in comparison with PAL technique. It is shown that adequate characterization methodology for free-volume defects in the modified spinel ceramics can be developed in terms of positron trapping model. The first component on the positron lifetime spectra has shown microstructure specificity of the spinel ceramics with octahedral and tetrahedral cation vacancies. The extended defects near grain boundaries (voids) are reflected by the second component. The small third component is due to “pick-off” annihilation of *o*-*Ps* in the intergranular nanopores. The observed *o*-*Ps* lifetime ~ 1.8 ns is related to the nanopores with radius of ~ 2.7 nm based on classic Tao-Eldrup equation. The reported data gives additional information to Hg-porosimetry and SEM results.

In the case of $\text{Cu}_{0.1}\text{Ni}_{0.8}\text{Co}_{0.2}\text{Mn}_{1.9}\text{O}_4$ ceramics, the results of PAL measurements confirm the interphase mass transfer processes caused by monolithization processes in ceramics during technological modification and owing to optimal content of additional NiO phase. Obtained results are in well agreement with microstructural X-ray diffractometry and electron microscopy data, confirming the structural changes in these ceramics caused by their technological modification.

Acknowledgments H. Klym thanks the Ministry of Education and Science of Ukraine for support (grant No 0116 U004411).

References

1. Salomao R, Bôas MOV, Pandolfelli VC (2011) Porous alumina-spinel ceramics for high temperature applications. *Ceram Int* 37(4):1393–1399 <https://doi.org/10.1016/j.ceramint.2011.01.012>
2. Feltz A, Pözl W (2000) Spinel forming ceramics of the system $\text{Fe}_x\text{Ni}_y\text{Mn}_{3-x-y}\text{O}_4$ for high temperature NTC thermistor applications. *J Eur Ceram Soc* 20(14):2353–2366 [https://doi.org/10.1016/S0955-2219\(00\)00140-0](https://doi.org/10.1016/S0955-2219(00)00140-0)
3. Feteira A (2009) Negative temperature coefficient resistance (NTCR) ceramic thermistors: an industrial perspective. *J Am Ceram Soc* 92(5):967–983. <https://doi.org/10.1111/j.1551-2916.2009.02990.x>

4. Shpotyuk O, Balitska V, Brunner M, Hadzaman I, Klym H (2015) Thermally-induced electronic relaxation in structurally-modified $\text{Cu}_{0.1}\text{Ni}_{0.8}\text{Co}_{0.2}\text{Mn}_{1.9}\text{O}_4$ spinel ceramics. *Phys B Condens Matter* 459:116–121 <https://doi.org/10.1016/j.physb.2014.11.023>
5. Klym H, Hadzaman I, Shpotyuk O (2015) Influence of sintering temperature on pore structure and electrical properties of technologically modified $\text{MgO-Al}_2\text{O}_3$ ceramics. *Mater Sci* 21(1):92–95 <https://doi.org/10.5755/j01.ms.21.1.5189>
6. Setter N (2001) Electroceramics: looking ahead. *J Eur Ceram Soc* 21(10):1279–1293. [https://doi.org/10.1016/S0955-2219\(01\)00217-5](https://doi.org/10.1016/S0955-2219(01)00217-5)
7. Rousset A, Tenaillieu C, Dufour P, Bordeneuve H, Pasquet I, Guillemet-Fritsch S, Schuurman S (2013) Electrical properties of $\text{Mn}_{3-x}\text{Co}_x\text{O}_4$ ($0 \leq x \leq 3$) ceramics: an interesting system for negative temperature coefficient thermistors. *Int J Appl Ceram Technol* 10(1):175–185. <https://doi.org/10.1111/j.1744-7402.2011.02723.x>
8. Bondarchuk A, Shpotyuk O, Glot A, Klym H (2012) Current saturation in In_2O_3 -SrO ceramics: a role of oxidizing atmosphere. *Revista mexicana de física* 58(4):313–316 <http://www.scielo.org.mx/pdf/rmf/v58n4/v58n4a5.pdf>
9. Deng ZY, Fukasawa T, Ando M, Zhang GJ, Ohji T (2001) Microstructure and mechanical properties of porous alumina ceramics fabricated by the decomposition of aluminum hydroxide. *J Am Ceram Soc* 84(11):2638–2644. <https://doi.org/10.1111/j.1151-2916.2001.tb01065.x>
10. Ohji T, Fukushima M (2012) Macro-porous ceramics: processing and properties. *Int Mater Rev* 57(2):115–131 <https://doi.org/10.1179/1743280411Y.0000000006>
11. Klym H, Ingram A, Shpotyuk O, Hadzaman I, Hotra O, Kostiv Y (2016) Nanostructural free-volume effects in humidity-sensitive $\text{MgO-Al}_2\text{O}_3$ ceramics for sensor applications. *J Mater Eng Perform* 25(3):866–873. <https://doi.org/10.1007/s11665-016-1931-9>
12. Shpotyuk O, Brunner M, Hadzaman I, Balitska V, Klym H (2016) Analytical description of degradation-relaxation transformations in nanoinhomogeneous spinel ceramics. *Nanoscale Res Lett* 11(1):499. <https://doi.org/10.1186/s11671-016-1722-0>
13. Klym H, Balitska V, Shpotyuk O, Hadzaman I (2014) Degradation transformation in spinel-type functional thick-film ceramic materials. *Microelectron Reliab* 54(12):2843–2848 <https://doi.org/10.1016/j.microrel.2014.07.137>
14. Krause-Rehberg R, Leipner HS (1999) Positron annihilation in semiconductors. *Defect studies*. Springer-Verlag, Berlin/Heidelberg/New York, p 378
15. Shpotyuk O, Filipecki J (2003) Free volume in vitreous chalcogenide semiconductors: possibilities of positron annihilation lifetime study. *Wyd-wo WSP w Czestochowie, Czestochowa*
16. Klym H, Ingram A, Shpotyuk O, Filipecki J, Hadzaman I (2011) Structural studies of spinel manganite ceramics with positron annihilation lifetime spectroscopy. *J Phys Conf Ser* 289(1):012010 <http://iopscience.iop.org/article/10.1088/1742-6596/289/1/012010/meta>
17. Klym H, Ingram A, Shpotyuk O, Filipecki J (2010) PALS as characterization tool in application to humidity-sensitive electroceramics. In: 27th international conference on microelectronics proceedings (MIEL), pp 239–242. <https://doi.org/10.1109/MIEL.2010.5490492>
18. Klym H, Ingram A, Shpotyuk O, Hadzaman I, Solntsev V (2016) Water-vapor sorption processes in nanoporous $\text{MgO-Al}_2\text{O}_3$ ceramics: the PAL spectroscopy study. *Nanoscale Res Lett* 11(1):1. <https://doi.org/10.1186/s11671-016-1352-6>
19. Shpotyuk O, Filipecki J, Ingram A, Golovchak R, Vakiv M, Klym H, Balitska V, Shpotyuk M, Kozdras A (2015) Positronics of subnanometer atomistic imperfections in solids as a high-informative structure characterization tool. *Nanoscale Res Lett* 10(1):1–5. <https://doi.org/10.1186/s11671-015-0764-z>
20. Klym H, Ingram A, Shpotyuk O, Hadzaman I, Solntsev V, Hotra O, Popov AI (2016) Positron annihilation characterization of free volume in micro-and macro-modified $\text{Cu}_{0.4}\text{Co}_{0.4}\text{Ni}_{0.4}\text{Mn}_{1.8}\text{O}_4$ ceramics. *Low Temp Phys* 42(7):601–605 <https://doi.org/10.1063/1.4959021>
21. Karbovnyk I, Bolesta I, Rovetskii I, Velgosh S, Klym H (2014) Studies of CdI_2 - Bi_3 microstructures with optical methods, atomic force microscopy and positron annihilation spectroscopy. *Mater Sci Poland* 32(3):391–395. <https://doi.org/10.2478/s13536-014-0215-z>

22. Hadzaman I, Klym H, Shpotyuk O (2014) Nanostructured oxyspinel multilayers for novel high-efficient conversion and control. *Int J Nanotechnol* 11(9–10–11):843–853 <https://doi.org/10.1504/IJNT.2014.063793>
23. Bodak O, Akselrud L, Demchenko P, Kotur B, Mrooz O, Hadzaman I, Shpotyuk O, Aldinger L, Seifert H, Volkov S, Pekhnyo V (2002) Crystal structure and electrical properties of $\text{Cu}_{0.8}\text{Ni}_{0.1}\text{Co}_{0.2}\text{Mn}_{1.9}\text{O}_4$ electroceramics. *J. Alloys Compd* 347:14–23 [https://doi.org/10.1016/S0925-8388\(02\)00675-8](https://doi.org/10.1016/S0925-8388(02)00675-8)
24. Klym H, Shpotyuk O, Ingram A, Calvez L, Hadzaman I, Yu K, Ivanusa A, Chalyy D (2017) Influence of free volumes on functional properties of modified chalcogenide glasses and oxide ceramics. *Springer Proc Phys* 195:479–493 https://doi.org/10.1007/978-3-319-56422-7_36
25. Klym HI, Ivanusa AI, Kostiv YM, Chalyy DO, Tkachuk TI, Dunets RB, Vasylychshyn II (2017) Methodology and algorithm of multicomponent analysis of positron annihilation spectra for nanostructured functional materials. *J Nano Electron Phys* 9(3):03037-1-6. [https://doi.org/10.21272/jnep.9\(3\).03037](https://doi.org/10.21272/jnep.9(3).03037)
26. Kansy J (1996) Microcomputer program for analysis of positron annihilation lifetime spectra. *Nucl Instrum Methods Phys Res, Sect A* 374(2):235–244 [https://doi.org/10.1016/0168-9002\(96\)00075-7](https://doi.org/10.1016/0168-9002(96)00075-7)
27. Klym H, Ingram A (2007) Unified model of multichannel positron annihilation in nanoporous magnesium aluminate ceramics. *J Phys Conf Ser* 79(1):012014 <https://doi.org/10.1088/1742-6596/79/1/012014>
28. Nambissan PMG, Upadhyay C, Verma HC (2003) Positron lifetime spectroscopic studies of nanocrystalline ZnFe_2O_4 . *J Appl Phys* 93:6320 <https://doi.org/10.1063/1.1569973>
29. Filipecki J, Ingram A, Klym H, Shpotyuk O, Vakiv M (2007) Water-sensitive positron-trapping modes in nanoporous magnesium aluminate ceramics. *J Phys Conf Ser* 79(1):012015. <https://doi.org/10.1088/1742-6596/79/1/012015>
30. Hassan HE, Sharshar T, Hessien MM, Hemeda OM (2013) Effect of γ -rays irradiation on Mn–Ni ferrites: structure, magnetic properties and positron annihilation studies. *Nucl Instrum Methods Phys Res, Sect B* 304:72–79. <https://doi.org/10.1016/j.nimb.2013.03.053>
31. Klym H, Ingram A, Shpotyuk O, Filipecki J, Hadzaman I (2010) Extended defects in insulating MgAl_2O_4 ceramic materials studied by PALS methods. *IOP Conf Ser Mater Sci Eng* 15(1):012044. <https://doi.org/10.1088/1757-899X/15/1/012044>
32. Jean YC, Mallon PE, Schrader DM (2003) Principles and application of positron and positronium chemistry. Word Scientific, Singapore
33. Mogensen OE (1995) Positron annihilation in chemistry. Springer, Berlin
34. Nakanishi H, Jean YC, Schrader DM, Jean YC (1998) In positron and positronium chemistry. Elsevier, Amsterdam
35. Dlubek G, Sen Gupta A, Pionteck J, Hassler R, Krause-Rehberg R, Kaspar H, Lochhaas KH (2005) High-pressure dependence of the free volume in fluoroelastomers from positron lifetime and PVT experiments. *Macromolecules* 38(2):429–437. <https://doi.org/10.1021/ma048310f>
36. Tao SJ (1972) Positronium annihilation in molecular substance. *J Chem Phys* 56(11):5499–5510 <https://doi.org/10.1063/1.1677067>
37. Eldrup M, Lightbody D, Sherwood JN (1981) The temperature dependence of positron lifetimes in solid pivalic acid. *Chem Phys* 63:51–58 [https://doi.org/10.1016/0301-0104\(81\)80307-2](https://doi.org/10.1016/0301-0104(81)80307-2)